Synthesis, Characterization and Investigation of Hydroxyapatite Powder

Rabiul Awal[a,b*], Md. Mostafa Raja[b], N.Y. Tanisa[a,b]

[a] *Department of Physics, Uttara University, Uttara, Dhaka-1230, Bangladesh*
[b] *Department of Physics, Jahangirnagar University, Dhaka-1342, Bangladesh*

Abstract

This study focuses on the synthesis and characterization of hydroxyapatite (HAP) using the precipitation method, investigating the influence of reaction conditions and heat treatment on its properties. Firstly, X-ray diffraction (XRD) analysis was conducted on synthesized HAP-1, comparing its data to standard HAP. The superior performance of HAP-2 (pH 11) over HAP-1 (pH 10.26) made it the preferred choice for final composite production. The stability of the hexagonal-dipyramidal phase within HAP-2 was observed even at elevated temperatures up to 1200°C, implying exceptional thermal stability. Fourier-transform infrared (FTIR) analysis provided insights into the molecular composition of HAP-2. The results underscore the potential to tailor HAP properties for various applications by controlling synthesis conditions and heat treatment parameters.

Keywords*:* Hydroxyapatite (HAP), calcium phosphate, X-ray diffraction (XRD), Fourier-transform infrared (FTIR)

1. Introduction

A calcium phosphate substance known as hydroxyapatite (HAP) plays a crucial role in various biological and medical applications due to its unique properties and biocompatibility [1-4]. It is a major component of natural bone and teeth, imparting structural integrity and strength to these tissues. Owing to its remarkable biocompatibility, HAP has found extensive use in biomaterials, tissue engineering, and medical implants [5-8]. Normally HAP is a family of calcium phosphate compounds and is a mineral constituent of bone. It is the hexagonal crystal structure of hydroxyapatite (HAP) in which calcium cations (Ca^{2+}) and phosphate anions (PO_4^{3-}) are settled around the pole of monovalent hydroxide anions [9] and pure HAP powder is white in color but naturally occurring apatite has different colors such as brown, yellow, etc. due to the incorporation of the various metal ions into the HAP crystal lattice [10].

In this research, we focus on the production, thorough identification, and investigation of HA powder. The synthesis methods may include precipitation, hydrothermal synthesis, sol-gel techniques, or other approaches, each with the potential to yield distinct HA properties. Furthermore, this research aims to explore the potential applications of the synthesized HA powder in areas such as bone regeneration, dental materials, drug delivery carriers, and bioactive coatings. By tailoring the synthesis parameters, we can potentially optimize the properties of HA powder to meet the specific requirements of these applications.

*Corresponding author
E-mail address: rabiulawal@uttarauniversity.edu.bd

2. Sample preparation

2.1 Sample collection

Sodium hydroxide [NaOH], ammonium dihydrogen phosphate [$NH_4H_2PO_4$], and calcium nitrate tetrahydrate [Ca $(NO_3)_2$+$4H_2O$] were acquired from Merck, India.

Fig. 1: (a) Calcium nitrate tetra-hydrate [Ca $(NO_3)_2$+$4H_2O$] powder, (b)Ammonium dihydrogen phosphate ($NH_4H_2PO_4$) powder, (c) Sodium hydroxide (NaOH) pellets

2.2 Preparation of Nano-sized HAP powder

Various techniques have been employed to synthesize hydroxyapatite (HAP), including the precipitation method [11-12]. In this method following process are required to prepare nanosized HAP powder. High-quality starting materials are chosen as precursors. These often include calcium sources (e.g., calcium nitrate, calcium chloride) and phosphate sources (e.g., ammonium dihydrogen phosphate) that provide the necessary ions for HAP formation. The precursors are dissolved in appropriate solvents, such as water or alcohol, to create a homogeneous solution. The molar ratio of calcium to phosphate is carefully controlled to promote the formation of HAP.

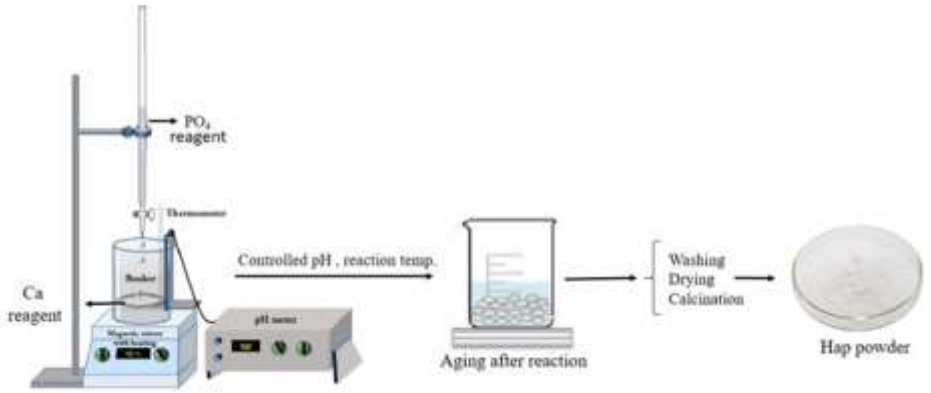

Fig. 2: The schematic diagram of HAP preparation.

The pH of the solution is adjusted to a specific range, usually slightly basic, to create favorable conditions for the nucleation and growth of HAP nanoparticles. The solution is heated or mixed under controlled conditions to initiate nucleation, where small clusters of HAP particles begin to form. As the process continues, these clusters grow into

nanosized HAP crystals. Techniques like hydrothermal synthesis or sol-gel methods are often employed to promote controlled nucleation and growth. Surfactants or stabilizing agents may be added to prevent particle agglomeration during the synthesis. After the desired particle size is achieved, the resulting nanosized HAP particles are separated from the solution through filtration or centrifugation. They are then thoroughly washed to remove any residual reagents or byproducts.

The washed nanosized HAP particles are carefully dried and subjected to calcination, which involves heating at elevated temperatures. This step aids in removing any remaining solvent and organic components while promoting crystal growth and crystallinity.

2.3 HAP synthesis

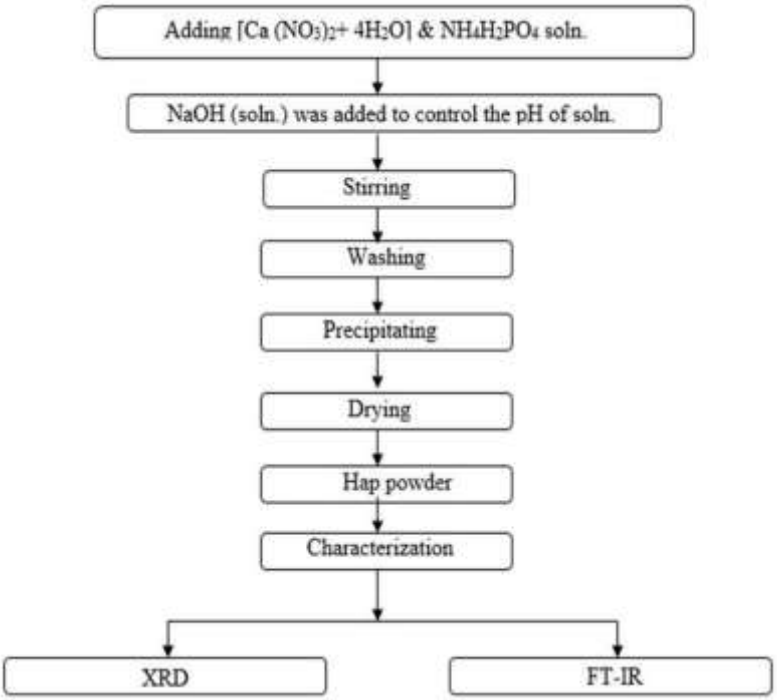

Fig. 3: Experimental flow diagram of HAP synthesis.

By using the chemical precipitation technique hydroxyapatite (HAP) was created. Here, agents for pH changes included a NaOH solution. In order to create 1M and 0.5M aqueous solutions, $[Ca(NO_3)_2+4H_2O]$ and $NH_4H_2PO_4$ were first dissolved and forcefully agitated in distilled water. The $[Ca(NO_3)_2+4H_2O]$ solution was continuously stirred at room temperature as drops of the $NH_4H_2PO_4$ aqueous solution were gently added. Following that, the pH was raised to 11 using the solution of sodium hydroxide (NaOH). The subsequent response provides an explanation for this:

$$10Ca\,(NO_3)_2{\cdot}4H_2O + 6NH_4H_2PO_4 + 8NaOH \rightarrow Ca_{10}\,(PO_4)_6(OH)_{\,2} + 20NaNO_3 + 20H_2O$$

The resultant solution was then agitated for the following at room temperature for 4 hours. After a whole day of aging before precipitation, the solution was filtered. Using pure water, the precipitated HAP was then repeatedly centrifuged for a half-hour at a speed of 12000 rpm. The resultant precipitate was dried at 40 to 55℃ before being calcined for an hour at 100, 450, 900, and 1200℃.

3. Result and discussion

3.1 . XRD data investigation

3.1.1 XRD study of HAP-1 and HAP-2

Figure 4 presents the XRD pattern of the produced HAP-1, and its data in Table 1 were compared to standard HAP data. The comparison revealed a strong resemblance between the synthesized HAP and the established HAP standard (Reference code: 01-086-0740), both in terms of d-spacing values and peak intensities. Notably, no impurity peaks were detected in the XRD pattern, affirming the dominance of the inorganic HAP phase. This outcome was consistent with a previous report [13]. The XRD analysis of HAP-1 powder disclosed a splitting of the Bragg peaks at (211) and (112), which satisfied Bragg's law through the simultaneous contact of the K vector with Ewald's sphere. Upon scrutinizing the XRD patterns of HAP-1 and HAP-2 samples, a key observation emerged: when the reaction pH fell below 10.30, the synthetic powder's XRD patterns diverged from standard hydroxyapatite patterns. Evidently, the pH of the reaction suspension played a pivotal role in determining HAP stability. Suboptimal pH levels (below 10.30) led to diminished crystallinity, as illustrated in Figure 4, while higher pH values promoted enhanced crystallinity. In light of chemical stability concerns, a higher pH was favored for HAP synthesis. HAP-2, which possessed a pH of 11, exhibited remarkable conformity to the common HAP powder (Ref. The Pattern: Hydroxyapatite, 01-086-0740), making it the preferred choice for the final composite production over HAP-1, which had a pH of 10.26.

Table 1: Comparison of XRD analysis among Standard HAP, HAP-1, and HAP-2

No.	plane	Standard HAP			HAP-1			HAP-2		
		d(A^0)	2θ(deg)	Peak intensity	d(A^0)	2θ(deg)	Peak intensity	d(A^0)	2θ(deg)	Peak intensity
1	002	3.44100	25.872	36.1	3.41508	26.0934	31.69	3.40781	26.1501	35.06
2	211	2.79695	31.973	100.0	2.78134	32.1842	100	2.79345	32.0409	100
3	112	2.77146	32.275	43.7	2.69755	33.2124	60.86	2.69755	33.2124	60.86
4	300	2.69969	33.157	54.3	2.71510	32.8940	70	2.71510	32.8940	70
5	202	2.62219	34.167	24.5	2.61510	34.2914	21.96	2.61510	34.2914	21.96
6	222	1.93385	46.947	24.8	1.93743	46.6891	17.05	1.93462	46.9683	40.01
7	213	1.83574	49.620	32.3	1.83487	49.6891	23.96	1.83478	49.6919	47.49
8	004	1.72050	53.195	13.5	1.71564	53.3672	16.43	1.71566	53.4044	23.19

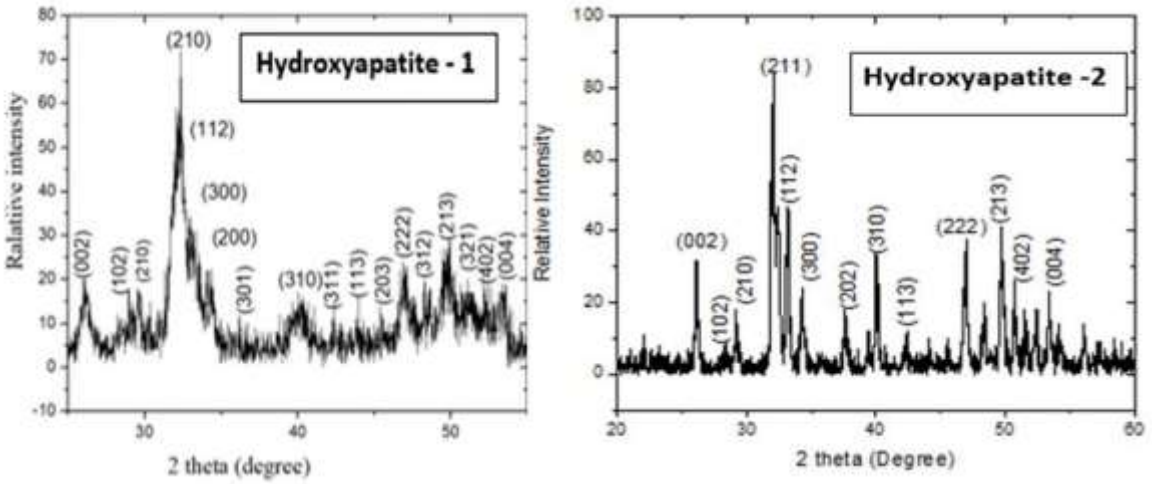

Fig. 4. The XRD pattern of synthesized HAP-1 and HAP-2.

3.1.2 XRD studies of HAP-2 powder heated at different temperatures

We examined the impact of heat treatment on phase changes and nano-crystallization in hydroxyapatite powder synthesized via the precipitation method. In Figure 5, we showcased the XRD pattern of hydroxyapatite powders (HAP-2) at various temperatures. The XRD phase analysis was based on the reference code Hydroxyapatite: 01-084-0740. It was evident that as the temperature increased, the peaks in the XRD patterns became sharper, indicating higher crystallinity at elevated temperatures.

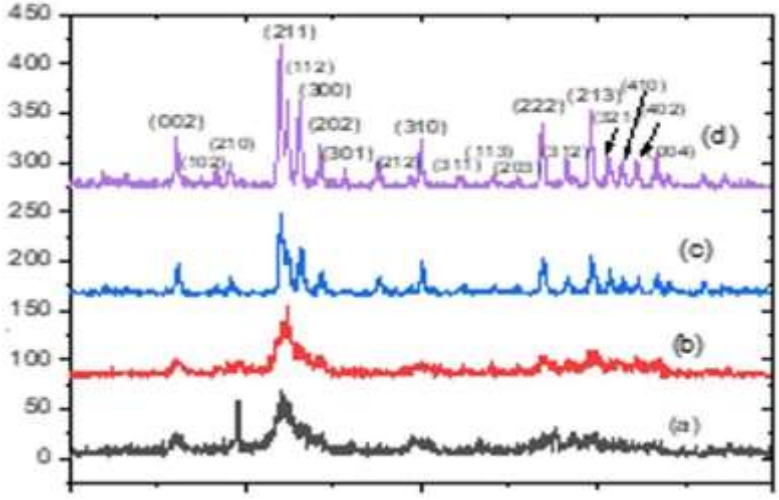

Fig. 5: XRD pattern of HAP-2 powder heated at different temperatures; (a) Room temperatures, (b) 450ºC, (c) 900ºC, (d) 1200ºC.

The presence of broad XRD lines indicated the nano-crystalline nature of the material. Initially, HAP-2 exhibited a stable hexagonal-dipyramidal phase at room temperature. Upon subjecting the sample to increasing temperatures, ranging from 100°C to 1200°C (with a 1-hour) were observed within the HAP-2 powder particles. Importantly, the hexagonal-dipyramidal phase remained unchanged up to 1200°C, without undergoing any phase transformation. At room temperature, the XRD peaks of HAP-2 showed limited resolution and intensity.Upon heat treatment at 450°C and 900°C, the XRD pattern of HAP-2 exhibited heightened intensity corresponding to planes around (211), (002),

(301), (222), and (213). However, no crystalline phase other than HAP was detected. This outcome concurred with the findings of Nazari et al. in 2014[13]. Notably, the XRD patterns of HAP-2 powders displayed a splitting of the Bragg peaks at (211) and (112), aligning with Bragg's law where the K vector intersects Ewald's sphere simultaneously.At temperatures of 1200°C, no new crystalline phases were observed in the HAP-2 sample.

3.2 FTIR analysis

3.2.1 FTIR absorption studies, sample HAP-2

We synthesized HAP-2 by employing calcium nitrate tetrahydrate [Ca $(NO_3)_2$•$4H_2O$] from Merck, Germany, and diammonium phosphate [$NH_4H_2PO_4$] from Loba Chemie, India, as precursors, maintaining a Ca/P ratio of 1.67. Two variations of hydroxyapatite, namely HAP-1 and HAP-2, were obtained based on different reaction pH values. However, for the final composite preparation, HAP-2 was utilized. The reaction pH during synthesis was set at 11. In Figure 6, we present the FTIR spectrum of the HAP-2 sample.

The appearance of broad bands at wave numbers 876 cm^{-1} and 1442 cm^{-1} indicates the incorporation of carbonate ions [14]. The carbonate-related bands are broad, encompassing contributions from surface carbonate ions, as seen in the literature for various HAP samples. We also detected two IR bands at approximately 2333 cm^{-1} and 2360 cm^{-1}, attributed to soluble CO^2 (g) within the ceramic material, although these are not shown in Figure 6. Broad bands observed at 1646 cm-1 and 3418 cm-1 signify the presence of adsorbed water in the material. Characteristic bands for the PO_4^{3-} ion are evident at 564 cm^{-1}, 612 cm^{-1}, and 1064 cm^{-1}. Notably, the v^3 band at 1039 cm^{-1} is particularly intense, while the v^2 band at 612 cm^{-1} is of medium intensity [15]. The bands spanning 900 cm^{-1} to 1200 cm^{-1} correspond to the stretching mode of the PO_4 group. The well-defined peaks at 564 cm^{-1} (v^4 band) and 612 cm^{-1} correspond to the bending vibration of PO_4 in hydroxyapatite [16].

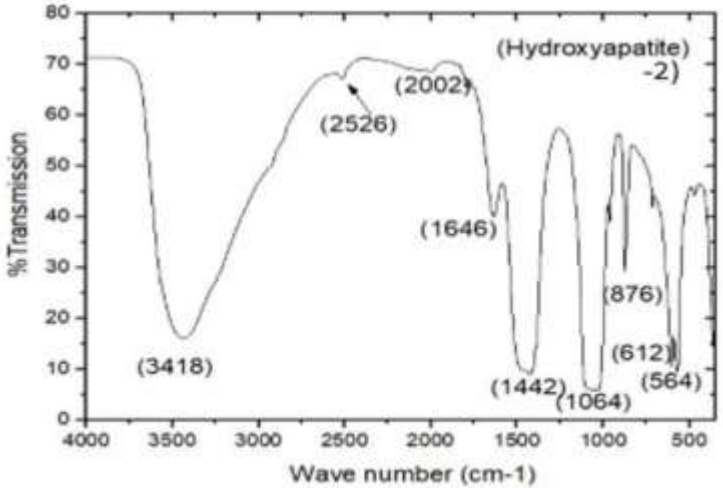

Fig. 6: FTIR spectrum of HAP-2 powder

3.2.2 FTIR absorption of HAP-2 sample at different temperatures

Here we see that at high temperatures, absorbed water molecules were vapored from the sample HAP-2. There were no peaks which are diminished at high temperatures, only the peak intensity of functional groups was decreased. So it was implied that at high temperatures, the crystallization and purity of the HAP-2 sample were increased [17-18].

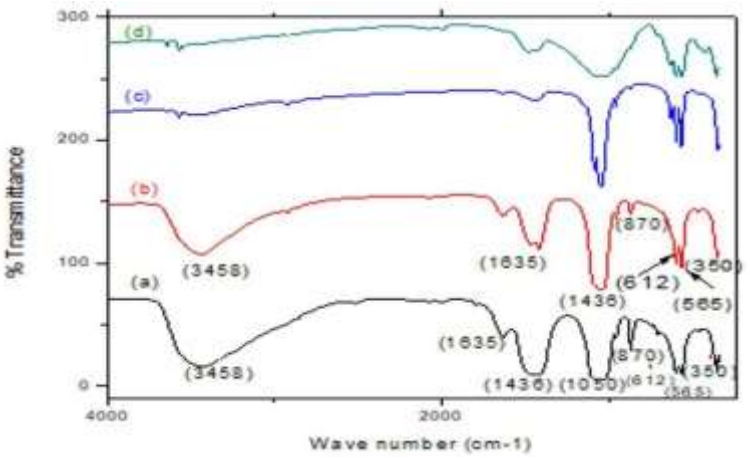

Fig. 7: Shows the FTIR spectrum of the HAP-2 sample at (a) room temperature (b) 450ºC (c) 900ºC and (d) 1200ºC.

Conclusions

HAP samples were synthesized by using calcium nitrate tetra-hydrate and ammonium di-hydrogen phosphate precursor chemicals at pH value 11. Initially, the XRD patterns of the synthesized HAP-1 were compared to standard HAP data, revealing a strong similarity in d-spacing values and peak intensities. The absence of impurity peaks corroborated the dominance of the inorganic HAP phase, consistent with previous research. Further XRD analysis of HAP-1 uncovered a notable splitting of Bragg peaks at (211) and (112), demonstrating compliance with Bragg's law through the simultaneous intersection of the K vector and Ewald's sphere. A pivotal role of reaction pH in influencing HAP stability was evident, where pH values below 10.30 led to decreased crystallinity, while higher pH values facilitated enhanced crystallinity. Consequently, a higher pH was favored for HAP synthesis, with HAP-2 (pH 11) selected for the production of final composites. Upon subjecting HAP-2 to heat treatment, XRD patterns revealed increased crystallinity as the temperature rose, with broad lines indicating a nano-crystalline nature. The stability of the hexagonal-dipyramidal phase within HAP-2 was confirmed, as it persisted even at elevated temperatures up to 1200°C. The impact of temperature on crystallinity and phase transformation was elucidated, emphasizing the critical role of heat treatment in enhancing material properties.FTIR analysis of HAP-2 unveiled insightful information about its molecular composition. The results highlight the potential of controlled synthesis and heat treatment in tailoring the crystallinity and phase composition of HAP for various applications.

Acknowledgments

The authors appreciate Dr. Md. Mahbubul Haque, Chief Scientific Officer, for his kind assistance during this research at the Materials Science Division, Atomic Energy Centre, Dhaka-1000, Bangladesh.

Conflicts of Interest

The authors declare no conflicts of interest.

References

1. Hou, X., Zhang, L., Zhou, Z., Luo, X., Wang, T., Zhao, X., Lu, B., Chen, F. and Zheng, L., 2022. Calcium phosphate-based biomaterials for bone repair. *Journal of functional biomaterials*, *13*(4), p.187.
2. Sathiyavimal, S., Vasantharaj, S., LewisOscar, F., Pugazhendhi, A. and Subashkumar, R., 2019. Biosynthesis and characterization of hydroxyapatite and its composite (hydroxyapatite-gelatin-chitosan-fibrin-bone ash) for bone tissue engineering applications. *International journal of biological macromolecules*, *129*, pp.844-852.
3. Lin, K. and Chang, J., 2015. Structure and properties of hydroxyapatite for biomedical applications. In *Hydroxyapatite (HAp) for biomedical applications* (pp. 3-19). Woodhead Publishing.
4. Prakasam, M., Locs, J., Salma-Ancane, K., Loca, D., Largeteau, A. and Berzina-Cimdina, L., 2015. Fabrication, properties and applications of dense hydroxyapatite: a review. *Journal of functional biomaterials*, *6*(4), pp.1099-1140.

5. Kareem, R.O., Bulut, N. and Kaygili, O., 2024. Hydroxyapatite biomaterials: a comprehensive review of their properties, structures, medical applications, and fabrication methods. *Journal of Chemical Reviews*, *6*(1), pp.1-26.
6. Islam, M.S., Abdulla-Al-Mamun, M., Khan, A. and Todo, M., 2020. Excellency of hydroxyapatite composite scaffolds for bone tissue engineering. *Biomaterials*, *10*, pp.1-22.
7. Osuchukwu, O.A., Salihi, A., Abdullahi, I., Abdulkareem, B. and Nwannenna, C.S., 2021. Synthesis techniques, characterization and mechanical properties of natural derived hydroxyapatite scaffolds for bone implants: A review. *SN Applied Sciences*, *3*, pp.1-23.
8. Szcześ, A., Hołysz, L. and Chibowski, E., 2017. Synthesis of hydroxyapatite for biomedical applications. *Advances in colloid and interface science*, *249*, pp.321-330.
9. Tolmacheva, N., Bhattacharyya, A. and Noh, I., 2024. Calcium Phosphate Biomaterials for 3D Bioprinting in Bone Tissue Engineering. *Biomimetics*, *9*(2), p.95.
10. Filip, D.G., Surdu, V.A., Paduraru, A.V. and Andronescu, E., 2022. Current development in biomaterials—hydroxyapatite and bioglass for applications in biomedical field: a review. *Journal of Functional Biomaterials*, *13*(4), p.248.
11. Abraham, A., Sharan Kumar, M., Anju Krishna, D. and Suba Sri, M., 2023. Development of nano-hydroxyapatite membrane using Momordica charantia and study of its biodegradability for medical application. *Biomass Conversion and Biorefinery*, pp.1-13.
12. Mehta, D., George, S. and Mondal, P., 2014. Synthesis of hydroxyapatite by chemical precipitation technique and study of its biodegradability. *International Journal of Research in Advent Technology*, *2*(4), pp.159-161.
13. Nazari, M., Ghasemi, N., Maddah, H. and Motlagh, M.M., 2014. Synthesis and characterization of maghemite nanopowders by chemical precipitation method. *Journal of Nanostructure in Chemistry*, *4*, pp.1-5.
14. Kumar, K.V., Subha, T.J., Ahila, K.G., Ravindran, B., Chang, S.W., Mahmoud, A.H., Mohammed, O.B. and Rathi, M.A., 2021. Spectral characterization of hydroxyapatite extracted from Black Sumatra and Fighting cock bone samples: A comparative analysis. *Saudi journal of biological sciences*, *28*(1), pp.840-846.
15. Ding, D., Yu, T., Zhang, W., Liu, W. and Huang, Y., 2015. Enhanced nanohydroxyapatite formation using a hydrolyzed gelatin. *Journal of nanomaterials*, *16*(1), pp.437-437.
16. Cahyaningrum, S.E., Herdyastuty, N., Devina, B. and Supangat, D., 2018, January. Synthesis and characterization of hydroxyapatite powder by wet precipitation method. In *IOP Conference Series: Materials Science and Engineering* (Vol. 299, p. 012039). IOP Publishing.
17. Zarif, M.E., Yehia-Alexe, S.A., Bita, B., Negut, I., Locovei, C. and Groza, A., 2022. Calcium phosphates–chitosan composite layers obtained by combining radio-frequency magnetron sputtering and matrix-assisted pulsed laser evaporation techniques. *Polymers*, *14*(23), p.5241.
18. Osuchukwu, O.A., Salihi, A., Abdullahi, I. and Obada, D.O., 2022. Experimental data on the characterization of hydroxyapatite produced from a novel mixture of biowastes. *Data in Brief*, *42*, p.108305.